# Identification of Parameters Influencing the Vascular Structure Displacement in Fusion Imaging during Endovascular Aneurysm Repair

Florent Lalys, Alexandre Barré, Moundji Kafi, Mohamed Benziane, Blandine Saudreau, Catherine Dupont, Adrien Kaladji

# Identification of parameters influencing the vascular structure displacement in fusion imaging during EVAR

Florent Lalys [1], Alexandre Barré [4], Moundji Kafi [4], Mohamed Benziane [1], Blandine Saudreau [4], Claire Dupont [2,3], Adrien Kaladji [2,3,4]

1. Therenva, F-35000, Rennes, France
2. INSERM, U1099, F-35000 Rennes, France
3. University Rennes 1, Signal and Image Processing Laboratory (LTSI), F-35000 Rennes, France
4. CHU Rennes, Department of Cardiothoracic and Vascular Surgery, F-35033 Rennes, France

## Abstract

**Purpose**. To quantify the displacement of the vascular structures after insertion of stiff devices during endovascular aneurysm repair (EVAR) of abdominal aortic aneurysm, and to identify potential parameters influencing this displacement.

**Materials and Methods**. A total of 50 patients from a single center undergoing EVAR were prospectively enrolled between January 2016 and December 2017. Fusion imaging was employed using the EndoNaut® (Therenva, France) station through a 3D/2D technology synchronizing the 3D CT-scan to the live intraoperative fluoroscopy. The accuracy of the fusion road-map was evaluated before deployment by conventional digital subtraction angiogram on a single plane (with different C-arm incidences).

**Results**. The mean displacement error of the ostium of the lowest renal artery was 4.1 +/- 2.4 mm (range 0 – 11.7 mm), with a left/right displacement of 1.6 +/- 1.7 mm (range 0 – 6.9 mm) and a craniocaudal displacement of 3.5 +/- 2.4 mm (range 0 – 11.3 mm). The correction required for the ostium of the lower renal artery was mostly cranial and to the left. Multiple linear regression analysis revealed only the sharpest angle between the aneurysm neck and sac as the factor influencing the accuracy of fusion imaging. All other parameters didn't show any correlation.

**Conclusion**. This study identified the sources of fusion error after insertion of rigid material during EVAR. As the sharpest angulation between aneurysm neck and sac increases, the overall accuracy of the fusion might be affected.

## Introduction

Fusion imaging during endovascular aortic interventions has gained attention recently, and is now accepted as a standard practice. With the increased complexity of aortic procedures, the volume of iodinated contrast used can increase, and reducing the amount of contrast is relevant because of its potentially nephrotoxic effects in patients with renal failure (1). For standard and complex EVAR, two types of systems are currently being used for fusion imaging. Historically, fusion was used using 3-dimensional (3D) to 3D co-registration workflow combining preoperative CTA and intraoperative cone-beam CT (CT) to guide the procedure. With a rotational acquisition realized at the beginning of the operation, registration can be used to align the preoperative and intraoperative coordinate systems (2–4). More recently, data matching has been done by 3D/2D registration based on intraoperative images (5–10) without the need of a rotational acquisition and with registration algorithms that can be used continuously during the procedure. For this new type of workflow, removing CBCT from the process of fusion imaging may have the benefit of decreasing the radiation dose while continuing to provide accurate image guidance. In both cases, published studies, reviewed in the recent meta-analysis of Goudeketting et al. (3), have shown that such augmented reality systems are capable of reducing the X-ray exposure time and the quantity of contrast agent injected. Specifically, use of 3D image fusion in standard and complex EVAR is associated with a significant decrease in contrast use, while radiation doses, procedure times, and fluoroscopy times are reduced in most studies, although not always significantly (4,11,12).

Despite proof that image fusion is effective for these procedures, its relevance is often questioned due to the deformation of vascular structure caused by the insertion of stiff devices (stiff wires and sheaths, stent graft delivery system) (3,7,8,11,13,14). Overlaid vascular

structures, segmented on the pre-operative CT-scan in case of 3D/2D workflow or on the CBCT in case of 3D/3D workflow, no longer reflect current arterial geometry as a result of the deformation caused by the introduction of tools of varying stiffness. This is the main source of errors in fusion systems, and accurate deployment of the stent graft still requires iterative injections of contrast agent before releasing each component of the stent graft. Initial studies showed that the displacement of renal arteries correlated to the aortic neck angles (7,11). However, stronger evidence of this correlation and identification of other potential clinical or anatomical parameters influencing the fusion error is needed. The primary objective of this study was to evaluate the displacement of renal ostia after insertion of a rigid system before deployment during EVAR. The second objective was to identify the potential parameters influencing this displacement.

## Material and Methods

### Study design and patient population

Between January 2016 and December 2017, 50 consecutive patients (84% men; mean age 74.2 years with range 57–90, mean BMI 28.5) undergoing EVAR (bifurcated stent grafts) in a single center were prospectively enrolled. Patients received Medtronic EnduRant II (40%), Cook Zenith Alpha Abdominal (40%), or Gore Excluder C3 (20%) stent grafts. The study was approved by the institutional ethics committee and all patients signed an informed consent form. Patients were not eligible for open repair, had an aneurysm diameter greater than 50 mm or had a growth rate greater than 1 cm per year. Patients operated with fenestrated or branched endografts, or ruptured aneurysms, were excluded. The CTAs were performed using a 64-slice scanner (General Electric Medical Systems, Milwaukee, Wisconsin, LightSpeed16), using a 215-260 mA, 120 kVp tube. 120 ml of a non-ionised iodine contrast medium (Hexabrix, Guerbet LLC, Bloomington, Ind) were injected. Procedures were performed in a

conventional operating room equipped with a mobile flat-panel detector (30*30 cm) (Cios-Alpha, Siemens®, Munich, Germany) and a floating table.
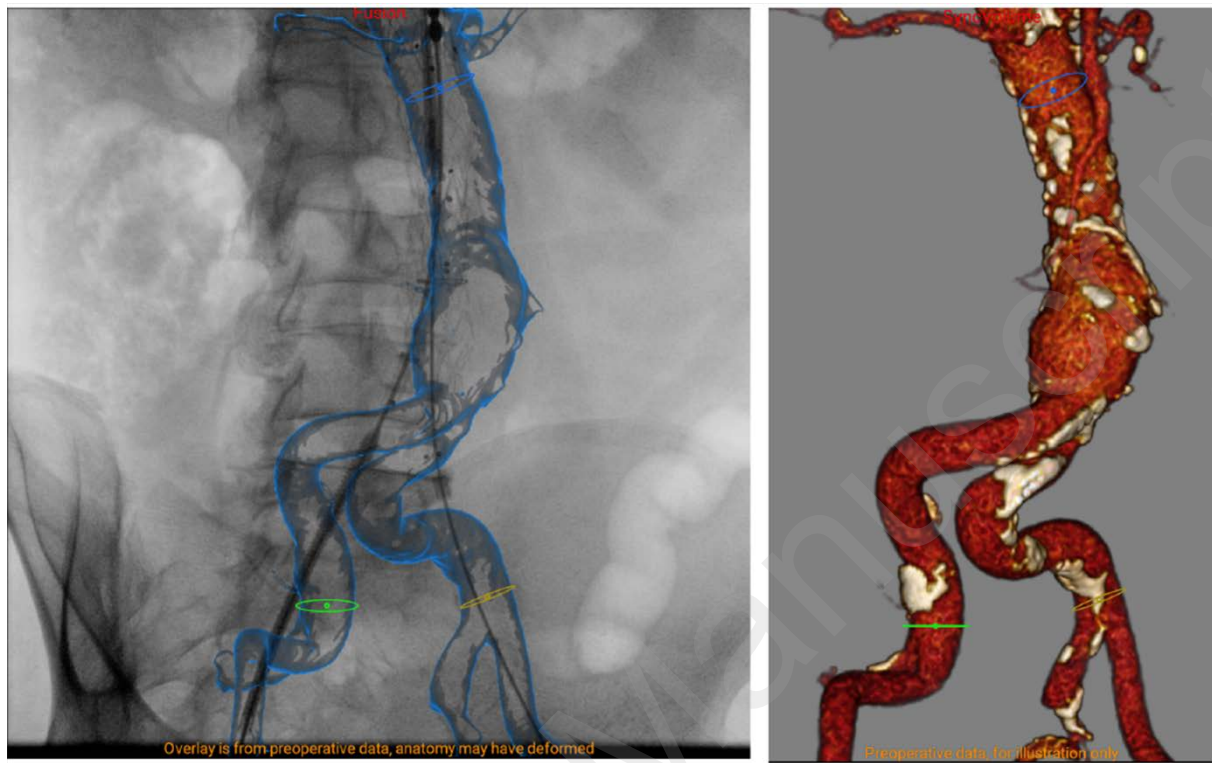


*Fig. 1. EndoNaut® station main screen visualization during an EVAR procedure, with the fusion overlaid on the fluoroscopic image on the left and the corresponding 3D visualization on the right. Circles represent the ostia of collaterals.*

**Fusion imaging workflow**

For each patient, fusion imaging was employed using the EndoNaut® (Therenva, France) station for navigation and positioning of the stent graft (12). Four surgeons participated in the study (2 junior surgeons with less than 5 years of experience and 2 senior surgeons with more than 10 years of experience). The EndoNaut® station has been designed to work with either mobile or fixed C-arm through a 3D/2D technology synchronizing the pre-operative 3D CTA to the live intraoperative fluoroscopy. The registration is performed with an intensity-based 3D/2D registration method that uses digitally reconstructed radiographs (DRR) computed from the bones mask of the 3D CTA. When needed, the 3D vascular segmentation and sizing landmarks can be shown in overlay on the 2D fluoroscopic image (Fig. 1). Compared to

3D/3D technologies, no CBCT is needed and only the available intraoperative fluoroscopy (with and without contrast injection, with and without the presence of endovascular tools) is required. The method is described in more detail in Duménil et al. (6).
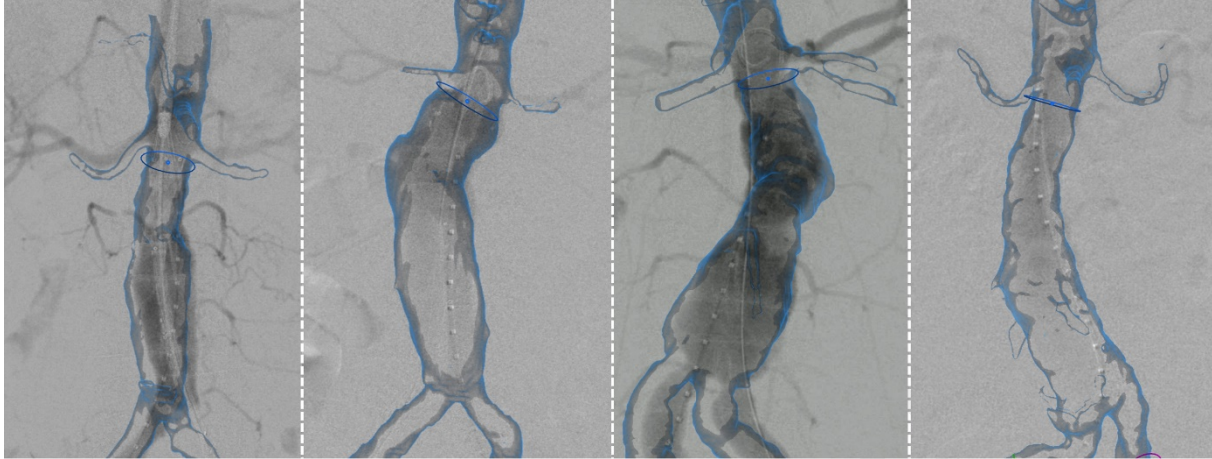


*Fig. 2. Example of fusion overlaid on the DSA before the correction step for 4 EVAR patients.*

Before deployment of each stent graft component, the accuracy of the fusion road-map was evaluated by conventional digital subtraction angiogram (DSA). The C-arm was used with different incidences, but with a maximum of 30° for both angulations. Each DSA was performed after the insertion of the delivery system, with the guidewire positioned in the ascending aorta (Lunderquist, Cook) and the delivery system as close as possible to the lowest renal artery. On the contralateral side, the angiogram was performed with a pigtail catheter. DSA was typically performed with a set dose of 10 ml to 30 ml, and all images (fluoroscopy and DSA) from the procedure were automatically recorded at native resolution using a video acquisition card. It allowed precisely computing the vascular structure displacement post-operatively, with the exact same images used during the operation (Fig. 2). After the 3D/2D registration on the bones structure, the displacement between the vascular structure displayed on the fusion and the vascular structure displayed on a single plane DSA was independently estimated by two experienced vascular surgeons. The displacements computed by both experts were averaged to be used for the analysis. All displacements (cranio-caudal and

left/right) were computed relative to patient position. The ostium of the lowest renal artery was used as reference for the correction.

**Anatomical analysis**

In addition to available demographic (age, gender, weight, BMI), imaging acquisition (CT slice thickness) and intervention (access route) data, a thorough quantitative analysis of each patient anatomy was performed with the EndoSize® software (Therenva, France) using the pre-operative CT-scan. A set of keypoints was manually positioned by the operator to segment the aorta and define the different anatomical zones (Fig. 3). The keypoints were positioned at the upper limit of the visible aorta on the CT-san (P1), below the lowest renal artery (P2), just above the aneurysm sac (P3), at the bifurcation level (P4), and at the right (P5) and left (P6) iliac bifurcation, respectively.
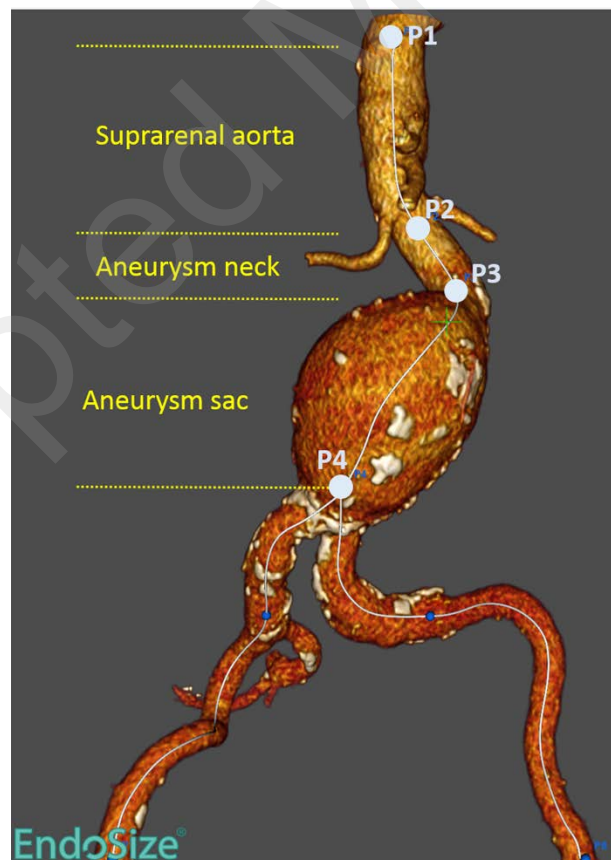


***Fig. 3.*** *Definition of the zones for anatomical parameters extraction.*

Definitions of preoperative variables were in accordance with the reporting standards of the Society for Vascular Surgery and the International Society for Cardiovascular Surgery (SVS/ISCS) (15). The tortuosity indexes were computed as the centerline length of the iliac segment divided by the length of the straight line. For the neck anatomy, the following variables were measured: aortic neck length (distance along the centerline between P2 and P3), proximal neck diameter (diameter perpendicular to the centerline at the level of P2), infrarenal and suprarenal neck angulation (angles between lines formed by P2-P3-P4 and P1-P2-P3, respectively), and proximal neck calcification (calcification grade between P2 and P3). For the aneurysm anatomy, the maximum diameter on a centerline view (mm) was extracted. The thrombus surrounding the aneurysm (i.e. between P3 and P4) was semi-automatically segmented using a homemade software. Information on the distance between the aorta and the spine was also estimated based on the segmentation of the bones and vascular structure (Fig. 4). Distance to bones (spine and pelvic bones) was computed at each point of the aorto-iliac volume surface (16). The map of the distances was then post-processed using MATLAB to analyze lumen wall to bones distance at different levels of the aorta.

For each iliac axis (i.e. between P4 and P5, and between P4 and P6 for the right and left iliac, respectively), the minimal diameter, the calcification grade and the tortuosity index were extracted. In light of recent studies highlighting the aorta angulation as the principal source of fusion errors (7,17), and in addition to the standard anatomical parameters usually extracted for EVAR planning, angulation-related parameters were extracted.

For each of the three zones (Fig. 3) defined by the proximal to distal keypoints P1 to P3 (suprarenal aorta and aneurysm neck), P2 to P4 (aneurysm neck and sac), and P1 to P4 (suprarenal aorta and aneurysm sac), the following were extracted: first, a number of points were defined along the centerline at different intervals (5, 10, 20 mm) to form straight lines, as explained by Dowson et al.(18). At each scale, the maximum angles computed between

adjacent line segments were extracted. Lastly, a standardized measure of the sharpest angulation, as defined by Van Keulen (19), was computed for the first two zones. Briefly, the 3D reconstruction of the vascular structure is turned 360 degrees perpendicular to the centerline in the middle of the flexure. The sharpest angle of the centerline is considered the true angle of the aortic axis.



***Fig. 4.*** *Visualization of the bone and vascular segmentation. Vascular color scale (blue to red) exhibits the vascular wall to bones distance map.*

**Statistical analysis**

Descriptive statistics, including means, standard deviations, ranges, and proportions, were calculated. Inter-observer variability was analyzed using the intraclass correlation coefficient (ICC). Univariate analyses were performed to investigate the influence of anatomical parameters on the vascular displacement at the level of the renal arteries. Pearson's correlation was preferred, without any covariate adjustment. The variables with a p-value <

0.05 were included in the multivariate analysis, which was subsequently performed using multiple linear regressions and a forward step-wise selection to identify best predictors. The fusion errors were plotted against aortic angulation. All statistical analyses were done using R software (The R foundation for statistical computing, 2009).

## Results

### Descriptive and univariate analysis

The ICC for interobserver variability was 0.98. The mean displacement error of the ostium of the lowest renal artery was 4.1 +/- 2.4 mm (range 0 – 11.7 mm), with a left/right displacement of 1.6 +/- 1.7 mm (range 0 – 6.9 mm) and a craniocaudal displacement of 3.5 +/- 2.4 mm (range 0 – 11.3 mm). The correction needed for renal arteries was cranial for 54 patients (98 %), along with a left correction for 23 patients (42%) and a right correction for 17 patients (31%). No demographic or usual sizing parameters influenced the displacement error, nor parameter related to the distance between the aorta and the spine (Table. 1.).

| Variable | Value | Correlation with total displacement (p-value of Pearson's correlation) |
|---|---|---|
| Age (in years) | 75.2 +/- 9.6 | 0.31 |
| Gender | 42 male, 8 female | 0.54 |
| Weight (in kg) | 83.6 +/- 15.8 | 0.71 |
| BMI | 28.5 +/- 4.6 | 0.69 |
| CT-scan slice thickness (in mm) | 0.7 +/- 0.2 | 0.39 |
| Access route | 39 right, 11 left iliac | 0.21 |
| Iliac tortuosity | 1.1 +/- 0.1 | 0.88 |
| Iliac calcification (grade) | 2.0 +/- 1.0 | 0.57 |
| Iliac minimal diameter (in mm) | 8.3 +/- 1.6 | 0.53 |
| Aortic neck length (in mm) | 26.6 +/- 14.3 | 0.72 |
| Proximal neck diameter (in mm) | 23.1 +/- 3.2 | 0.44 |
| Proximal neck calcification (grade) | 1.2 +/- 0.5 | 0.97 |
| AAA diameter (in mm) | 51.6 +/- 7.3 | 0.18 |
| Thrombus volume (in mm$^3$) | 43.6 +/- 37.3 | 0.71 |
| Distance to spine - P2 level (mm) | 28.0 +/- 17.4 | 0.43 |
| Distance to spine - P1 -> P4 | | |
|     Minimum (mm) | 0.4 +/- 0.4 | 0.33 |
|     Maximum (mm) | 12.3 +/- 18.7 | 0.54 |
|     Mean (mm) | 4.1 +/- 4.8 | 0.26 |

**Tab. 1.** *Descriptive statistics and correlation with total displacement error on renal arteries*

However, a large number of angle parameters computed from the suprarenal aorta and aneurysm neck and sac were strongly correlated with the displacement error from the univariate analysis (Table. 2).

| Variable | Value | Correlation with total displacement (p-value of Pearson's correlation) |
|---|---|---|
| Infrarenal neck angle (°) | 30.3 +/- 12.9 | **0.0002** |
| Suprarenal neck angle (°) | 19.1 +/- 13.3 | **0.0013** |
| | | |
| P1 -> P3 | | |
| Tortuosity index | 1.04 +/- 0.05 | **0.0394** |
| Max angle (scale = 5mm) (°) | 11.8 +/- 2.9 | 0.7018 |
| Max angle (scale = 10mm) (°) | 16.3 +/- 4.9 | 0.6660 |
| Max angle (scale = 20mm) (°) | 19.3 +/- 8.1 | 0.1389 |
| Sharpest angle (°) | 29.6 +/- 16.4 | **0.0319** |
| | | |
| P2 -> P4 | | |
| Tortuosity index | 1.09 +/- 0.05 | **0.0029** |
| Max angle (scale = 5mm) (°) | 20.1 +/- 10.0 | **0.0112** |
| Max angle (scale = 10mm) (°) | 23.9 +/- 8.2 | 0.1083 |
| Max angle (scale = 20mm) (°) | 30.4 +/- 12.7 | **0.0079** |
| Sharpest angle (°) | 44.6 +/- 12.8 | **< 0.0001** |
| | | |
| P1 -> P4 | | |
| Tortuosity index | 1.08 +/- 0.05 | **0.0049** |
| Max angle (scale = 5mm) (°) | 19.7 +/- 7.7 | **0.0120** |
| Max angle (scale = 10mm) (°) | 24.3 +/- 7.3 | **0.0406** |
| Max angle (scale = 20mm) (°) | 31.6 +/- 11.5 | **0.0388** |

**Tab. 2.** *Descriptive statistics and correlation with total displacement error on renal arteries (in bold, p-values < 0.05)*

**Multi-variate analysis**

Multiple linear regression analysis revealed only the sharpest angle between P2 and P4 as the factor influencing the accuracy of fusion imaging (p = 0.00001, Fig. 5). After including this parameter into the linear model, no other parameters can bring additional significant information.
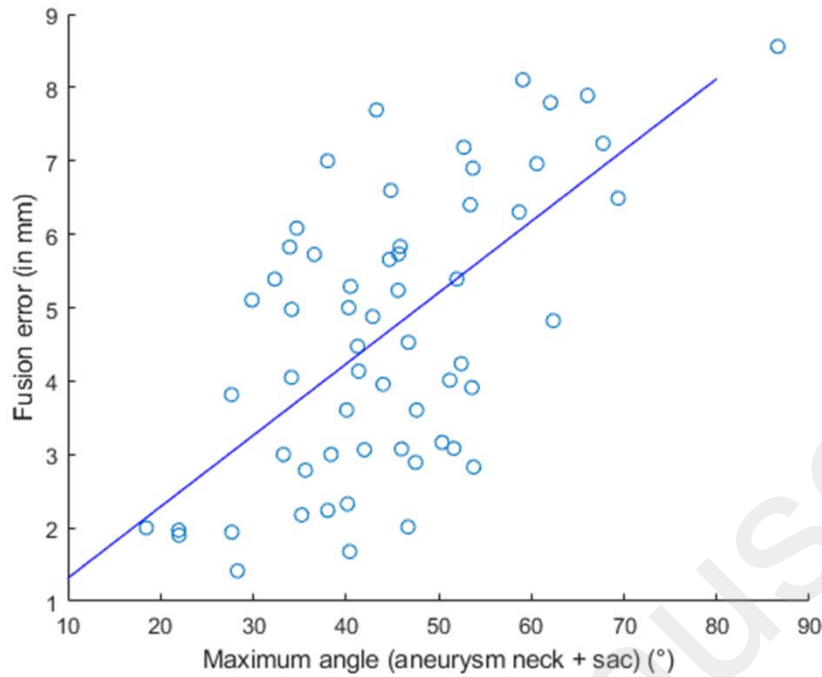
***Fig. 5.*** *Scatter plot of the total displacement error compared to the sharpest angle computed on the aneurysm neck + sac (i.e. between P2 and P4).*

## Discussion

In this study, a large number of anatomical variables were collected and their influence on the fusion error during EVAR was studied. Insertion of rigid material (stiff guidewires and delivery systems) leads to significant displacement of the aorta when compared to the preoperative CT scan, with a mean displacement error of 4.1 +/- 2.4 mm estimated at the level of the renal arteries. The only factor influencing this error was found to be the sharpest angle between the aneurysm sac and neck (p=0.00001).

There is a growing interest of image fusion systems in endovascular procedures, for complex cases but also recently routinely used for standard EVAR cases. Practical experience and precise knowledge of the limitations and sources of errors of this technology are of critical importance. In many papers it is currently recognized that vascular deformation induced by the guide wire and delivery device stiffness is the main limiting factor. These deformations

12

can have clinical consequences and must be accounted for, first at the planning step, and then, during the procedure.

The fusion error due to aortic deformation estimated in this series is consistent with other recent publications (4,7,8,13,14,17,20,21). Carrel et al. (7) have first emphasized the limitations of image fusion in the case of tortuous aortic necks. Their study on 11 EVAR cases demonstrated a mean error of 4.5 +/- 2.8 mm, with significantly higher deformation at the level of the renal ostia beyond angulation of 30°. A mean error at renal artery origin of 2.0 +/- 2.5 mm, (range from 0 - 7 mm), 3.9 mm (maximum 9.5 mm) and were reported by Fukuda et al. (8), Rolls et al. (4) and , respectively. Maurel et al. (13) reported similar findings , with an ostium displacement of 6.2 mm (range 2.5 – 13.5 mm) and 6.4 mm (range 1.9 – 14.5 mm) for the right and left renal arteries, respectively, with mostly left and superior displacements. On 101 EVAR patients, Schultz et al. (17) reported a total deviation of 6 mm (range 0 – 22 mm), including a craniocaudal deviation of 3 mm (range 0 – 15 mm). Koutouzi et al. (21), Kauffmann et al. (14) and Ahmad et al. (20) reported similar registration errors on relatively small series. Our study, using a dataset of 50 patients and advanced anatomical parameters, corroborates initial conclusions (7,17) that the displacement error is strongly correlated with the angulation of the aorta.  One explanation could be that the delivery system is mainly placed in this segment of the aorta and the stiffness will be maximum along the z-axis affecting therefore each parameter that modify the direction of the delivery system such as the infrarenal angulation. The volume of thrombus and the distance to the spine have no influence because they are factors maintaining the aorta in the lateral and antero-posterior axis and would be marginally modified by the presence of the delivery system. Moreover, the distance to the spine is computed from the arterial lumen and overestimates the real distance of the outer wall that is in most of the cases close to the spine. Compared to Schultz et al. (17), the CTA slice thickness was not found to influence the fusion error in our series.

Another potential source of error is the difference between the position of the patient's arms during CTA and during the procedure. Usually the arms rest on both sides during EVAR but are raised over the head during CTA to improve visualization and image quality, which may modify the position of the vascular structure with respect to the bones. A recent study, however, concluded that the displacement of the abdominal aorta (calculated from the anterior position) between elevated and non-elevated arms was non-significant (1.2 +/- 0.8 mm) (22). If this result still needs to be corroborated, the displacement induced by the position of the arms seems to be minor. Secondly, the respiratory movement can impact the position of the aorta, but the renal ostia are relatively fixed with a displacement < 2mm during respiratory cycle (23). Compensating the respiratory variation would therefore be probably unnecessary. The intraluminal thrombus, particularly in case of significant thickness, may also play a part in the behavior of the vascular structure (24,25), providing a rigidity to the wall which can slightly impact the position of the renal ostia.

Current fusion technology cannot compensate for the fusion error yet. In current practice, the superior and inferior movements of the renal arteries are determinant when it comes to avoiding renal coverage during deployment. Based on an average 6mm diameter of the renal artery ostium, the range of an acceptable clinical accuracy can be set to 3mm (7), which is lower than the average fusion error obtained in this study (> 4mm). Consequently, it is unsafe to release a component without performing a small contrast agent injection (14). This can be done by minimal contrast injection to identify the renal ostium with readjustment of the fusion imaging. In image fusion application, it is therefore important to be able to easily and rapidly manually correct this displacement to update the intraoperative overlay. Our data support the need for future fusion applications that take into account the fusion error and automatically update it, even if current status on this phenomena do not support a zero contrast procedure solely relying on fusion imaging so far. To address this problem, alternative strategies are also

possible. Works have focused on the question of taking into account intraoperative deformations using non-rigid registrations and biomechanical simulation models (26,27). When using numerical simulation, a deformed volume could be estimated prior to the procedure (16,27) and be used instead of the preoperative CT-scan for registration and visualization. If numerical simulation could be optimized for estimating the deformation of the iliac arteries, current models make strong hypothesis on the anchorage of the abdominal aorta are taken that does not allow for the displacement compensation at this level.

Some inevitable limitations can be observed. In this work, the fusion error was measured on a single 2D DSA without estimating the anteroposterior displacement, whereas the majority of images was acquired with different incidences (maximum of 30° for both C-arm angles). For correctly estimating anteroposterior displacement, the acquisition of a CBCT after the insertion of the material would be needed, but this will require additional radiation dose. An error on the anteroposterior dimension is not to be excluded, even if the use of a 2D overlay on fusion imaging systems temper the importance of this error. The estimation of the fusion error was performed by two experts (ICC = 0.98). It is in line with the work of Kauffmann et al. (14), which reported a very high inter-observer agreement for the measurements of renal artery displacement (ICC > 0.99).

## Conclusion

This study has tested the influence of anatomical parameters that could have an influence on the vascular displacement usually observed with fusion imaging during aortic endovascular procedures. As the sharpest angulation between aneurysm neck and sac increases, the overall accuracy of the fusion might be affected and is severe enough to preclude deployment without contrast imaging for validation.

# References

1.  Kawatani Y, Nakamura Y, Mochida Y, Yamauchi N, Hayashi Y, Taneichi T, et al. Contrast Medium Induced Nephropathy after Endovascular Stent Graft Placement: An Examination of Its Prevalence and Risk Factors [Internet]. Radiology Research and Practice. 2016 [cited 2018 Mar 26]. Available from: https://www.hindawi.com/journals/rrp/2016/5950986/

2.  Hertault A, Overbeck K, Sobocinski J, Azzaoui R, Fabre D, Haulon S. Recent developments in intraoperative imaging and navigation during aortic interventions. J Cardiovasc Surg (Torino). 2017 Jul 18;

3.  Goudeketting SR, Heinen SGH, Ünlü Ç, van den Heuvel DAF, de Vries J-PPM, van Strijen MJ, et al. Pros and Cons of 3D Image Fusion in Endovascular Aortic Repair: A Systematic Review and Meta-analysis. J Endovasc Ther Off J Int Soc Endovasc Spec. 2017 May 1;1526602817708196.

4.  Rolls AE, Maurel B, Davis M, Constantinou J, Hamilton G, Mastracci TM. A Comparison of Accuracy of Image- versus Hardware-based Tracking Technologies in 3D Fusion in Aortic Endografting. Eur J Vasc Endovasc Surg Off J Eur Soc Vasc Surg. 2016 Jul 4;

5.  Sailer AM, de Haan MW, Peppelenbosch AG, Jacobs MJ, Wildberger JE, Schurink GWH. CTA with fluoroscopy image fusion guidance in endovascular complex aortic aneurysm repair. Eur J Vasc Endovasc Surg Off J Eur Soc Vasc Surg. 2014 Apr;47(4):349–56.

6.  Duménil A, Kaladji A, Castro M, Göksu C, Lucas A, Haigron P. A versatile intensity-based 3D/2D rigid registration compatible with mobile C-arm for endovascular treatment of abdominal aortic aneurysm. Int J Comput Assist Radiol Surg. 2016 May 26;

7.  Carrell TWG, Modarai B, Brown JRI, Penney GP. Feasibility and Limitations of an Automated 2D-3D Rigid Image Registration System for Complex Endovascular Aortic Procedures. J Endovasc Ther. 2010;17(4):527–33.

8.  Fukuda T, Matsuda H, Doi S, Sugiyama M, Morita Y, Yamada M, et al. Evaluation of automated 2D-3D image overlay system utilizing subtraction of bone marrow image for EVAR: feasibility study. Eur J Vasc Endovasc Surg Off J Eur Soc Vasc Surg. 2013 Jul;46(1):75–81.

9.  Panuccio G, Torsello GF, Pfister M, Bisdas T, Bosiers MJ, Torsello G, et al. Computer-aided endovascular aortic repair using fully automated two- and three-dimensional fusion imaging. J Vasc Surg [Internet]. 2016 [cited 2016 Aug 31]; Available from: http://www.sciencedirect.com/science/article/pii/S0741521416308278

10. Tacher V, Lin M, Desgranges P, Deux J-F, Grünhagen T, Becquemin J-P, et al. Image guidance for endovascular repair of complex aortic aneurysms: comparison of two-dimensional and three-dimensional angiography and image fusion. J Vasc Interv Radiol JVIR. 2013 Nov;24(11):1698–706.

11. Schulz CJ, Schmitt M, Böckler D, Geisbüsch P. Fusion Imaging to Support Endovascular Aneurysm Repair Using 3D-3D Registration. J Endovasc Ther Off J Int Soc Endovasc Spec. 2016 Jul 25;

12. Kaladji A, Villena A, Pascot R, Lalys F, Daoudal A, Clochard E, et al. Fusion Imaging for EVAR with Mobile C-arm. Ann Vasc Surg [Internet]. 2018 Aug 6 [cited 2018 Oct 5]; Available from: http://www.sciencedirect.com/science/article/pii/S0890509618305843

13. Maurel B, Hertault A, Gonzalez TM, Sobocinski J, Le Roux M, Delaplace J, et al. Evaluation of Visceral Artery Displacement by Endograft Delivery System Insertion. J Endovasc Ther. 2014 Apr 1;21(2):339–47.

14. Kauffmann C, Douane F, Therasse E, Lessard S, Elkouri S, Gilbert P, et al. Source of errors and accuracy of a two-dimensional/three-dimensional fusion road map for endovascular aneurysm repair of abdominal aortic aneurysm. J Vasc Interv Radiol JVIR. 2015 Apr;26(4):544–51.

15. Chaikof EL, Blankensteijn JD, Harris PL, White GH, Zarins CK, Bernhard VM, et al. Reporting standards for endovascular aortic aneurysm repair. J Vasc Surg. 2002 May;35(5):1048–60.

16. Gindre J, Bel-Brunon A, Rochette M, Lucas A, Kaladji A, Haigron P, et al. Patient-Specific Finite-Element Simulation of the Insertion of Guidewire During an EVAR Procedure: Guidewire Position Prediction Validation on 28 Cases. IEEE Trans Biomed Eng. 2017 May;64(5):1057–66.

17. Schulz CJ, Schmitt M, Böckler D, Geisbüsch P. Feasibility and accuracy of fusion imaging during thoracic endovascular aortic repair. J Vasc Surg [Internet]. 2015 Oct 29; Available from: http://www.jvascsurg.org/article/S0741-5214(15)01839-X/abstract

18. Dowson N, Boult M, Cowled P, De Loryn T, Fitridge R. Development of an Automated Measure of Iliac Artery Tortuosity that Successfully Predicts Early Graft-Related Complications Associated with Endovascular Aneurysm Repair. Eur J Vasc Endovasc Surg. 2014 Aug;48(2):153–60.

19. van Keulen JW, Moll FL, Tolenaar JL, Verhagen HJM, van Herwaarden JA. Validation of a new standardized method to measure proximal aneurysm neck angulation. J Vasc Surg. 2010 Apr;51(4):821–8.

20. Ahmad W, Obeidi Y, Majd P, Brunkwall JS. The 2D-3D registration method in Image Fusion is accurate and helps to reduce the used contrast medium, radiation and procedural time in standard EVAR procedures. Ann Vasc Surg. 2018 Mar 6;

21. Koutouzi G, Sandström C, Roos H, Henrikson O, Leonhardt H, Falkenberg M. Orthogonal Rings, Fiducial Markers, and Overlay Accuracy When Image Fusion is Used for EVAR Guidance. Eur J Vasc Endovasc Surg Off J Eur Soc Vasc Surg. 2016 Sep 7;

22. Doyle MG, Roy D, Kauffmann C, Tan KT, Soulez G, Amon CH, et al. Arm elevation during computed tomography does not significantly alter abdominal aortic aneurysm anatomy. Diagn Interv Imaging. 2017 Mar 1;98(3):279–82.

23. Draney MT, Zarins CK, Taylor CA. Three-dimensional analysis of renal artery bending motion during respiration. J Endovasc Ther. 2005;12(3):380–386.

24. Riveros F, Martufi G, Gasser TC, Rodriguez JF. Influence of intraluminal thrombus topology on AAA passive mechanics. Comput Cardiol Conf CinC 2013. 2013 Sep 22;899–902.

25. Wang DHJ, Makaroun MS, Webster MW, Vorp DA. Effect of intraluminal thrombus on wall stress in patient-specific models of abdominal aortic aneurysm. J Vasc Surg. 2002 Sep;36(3):598–604.

26. Guyot A, Varnavas A, Carrell T, Penney G. Non-rigid 2D-3D registration using anisotropic error ellipsoids to account for projection uncertainties during aortic surgery. Med Image Comput Comput-Assist Interv MICCAI Int Conf Med Image Comput Comput-Assist Interv. 2013;16(Pt 3):179–86.

27. Duménil A, Kaladji A, Castro M, Esneault S, Lucas A, Rochette M, et al. Finite-element-based matching of pre- and intraoperative data for image-guided endovascular aneurysm repair. IEEE Trans Biomed Eng. 2013 May;60(5):1353–62.